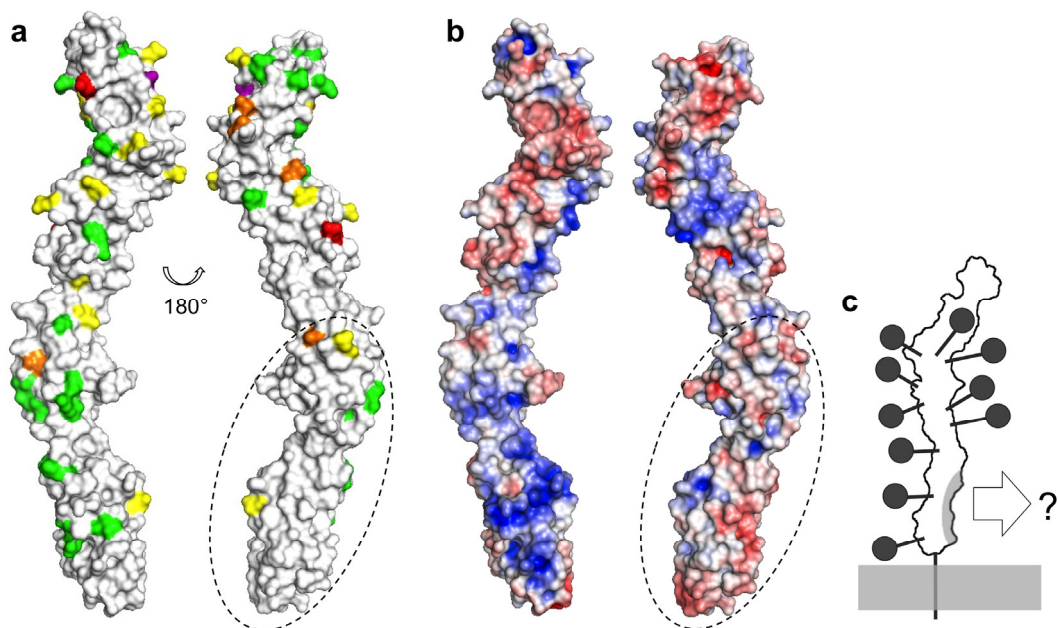


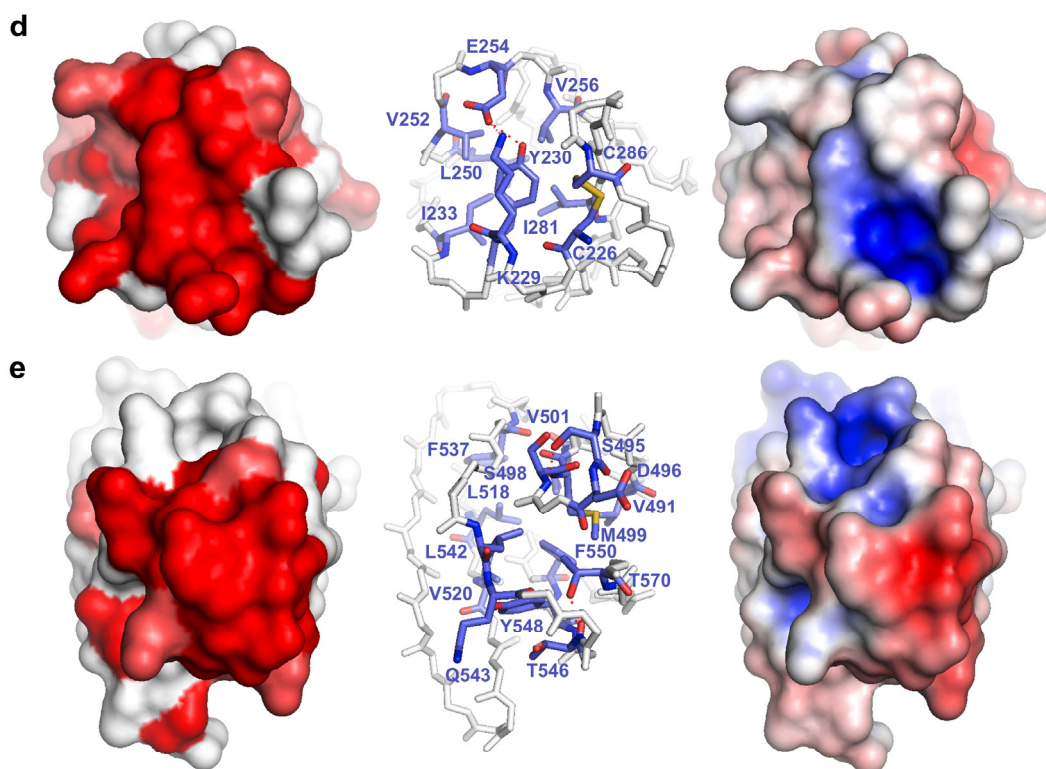
## Supplementary Figure 1

### Proteins used in the study and representative electron density.

**(a)** (Left) N-glycosylated proteins analyzed using MALS (lanes 1–3), cryo-EM (lane 4) and VA-TIRF (lanes 5–7): CD45RABC (lane 1), CD45R0 (lane 2), CD45d1–d4 (lane 3) and Sema6A-CD45R0 (lane 4), and N-terminally HaloTag-tagged forms of CD45RABC (lane 5), CD45R0 (lane 6) and CD45d1–d4 (lane 7). Top and bottom panels show 10% non-reducing (NR) and reducing (R) SDS-PAGE gels, respectively. (Right) Endo F1-deglycosylated proteins used for growing crystals: CD45d1–d4 (lane 1), CD45d1–d3 (lane 2), CD45d1d2 (lane 3) and rCD45d3d4 (lane 4). Top and bottom panels show 15% NR and R SDS-PAGE gels, respectively. **(b)** Electron density maps for CD45d1d2. **(i)** KPtCl<sub>4</sub>-SAD phased, phase-extended and density modified map from SHARP (calculated to 2.3 Å and contoured at 1.1 σ). The two CD45d1d2 molecules in the crystallographic asymmetric unit are colored yellow and magenta, respectively. **(ii–iii)** Close-up view of the density for the residual GlcNAc (remaining following Endo F1 cleavage of N-linked oligosaccharides) at residue N378. In **(ii)**, a region of the experimental map in **(i)** is shown. In **(iii)**, the SigmaA-weighted 2Fo-Fc map of the final refinement step from autoBUSTER, calculated to 2.3 Å resolution and contoured at 1.1 σ is shown. **(c)** rCD45d3d4 maps. **(i)** Ta<sub>6</sub>Br<sub>12</sub>-SAD phased, phase-extended and density modified map from SHARP (calculated to 2.45 Å and contoured at 1.1 σ). The two rCD45d3d4 molecules in the crystallographic asymmetric unit are colored yellow and magenta, respectively. **(ii–iii)** Close-up view of electron density for the residual GlcNAc at residue N502. In **(ii)**, a region of the experimental map in **(i)** is shown. In **(iii)**, the SigmaA-weighted 2Fo-Fc map of the final refinement from autoBUSTER, calculated to 2.45 Å resolution contoured at 1.1 σ is shown. **(d)** CD45d1–d4 maps. **(i–ii)** Stick representation of the final CD45d1–d4 model showing the two molecules in the asymmetric unit. **(i)** SigmaA-weighted 2Fo-Fc map of the final refinement step from autoBUSTER contoured at 1.0 σ. The model is in atomic colouring (oxygen: red; nitrogen: blue; sulphur: orange; carbon: yellow/red). In **(ii)** the two CD45d1–d4 molecules per asymmetric unit are colour-coded according to temperature factors (green, low B and red, high B).



Conserved in: 4-5/11 sequences  
 7/11 sequences 2-3/11 sequences  
 6/11 sequences One sequence only

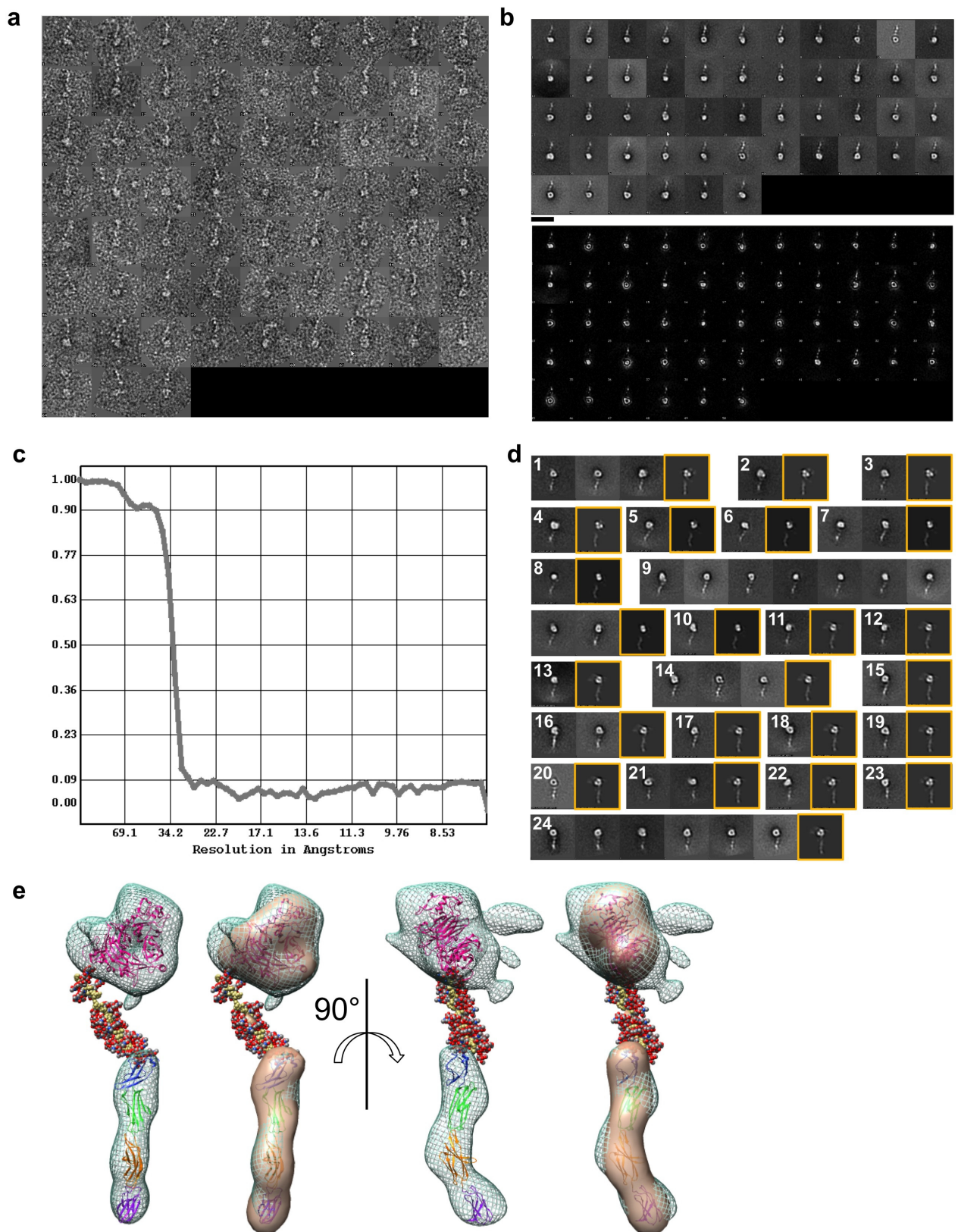


## Supplementary Figure 2

### Glycosylation and conservation at the 'top' and base of the modular region of CD45.

(**a**) Thirteen animal CD45 sequences were aligned using MULTALIN (data not shown). Glycosylation sequons in these sequences were identified using NetNGlyc, and the putatively glycosylated Asn-equivalent positions mapped onto the human CD45d1–d4 crystal structure using the alignment. Sites were colored according to conservation level using the alignment. (**b**) Electrostatic potential calculated using PyMol ( $-5 \text{ K}_b\text{T}/e_c$  (red) to  $+5 \text{ K}_b\text{T}/e_c$  (blue)) is shown. This analysis identifies a surface with asymmetric charge and N-glycan distribution perhaps used to access substrates (shaded region in **c**). Views of the d1–d4 region along its long axis from the top (**d**) and bottom (**e**) depict: (*left*) residue conservation at the top and base (residues are colored according to the number of identical or conservatively substituted residues at each position in an alignment of 11 mammalian sequences (data not shown; see Online Methods for residue groupings)); (*middle*) the network of conserved residues forming the caps (purple, shown in stick format); and (*right*) the surface electrostatic potential calculated using PyMol ( $-5 \text{ K}_b\text{T}/e_c$  (red) to  $+5 \text{ K}_b\text{T}/e_c$  (blue)). For the sake of clarity, the middle panels in d,e are drawn slightly enlarged relative to the other panels.

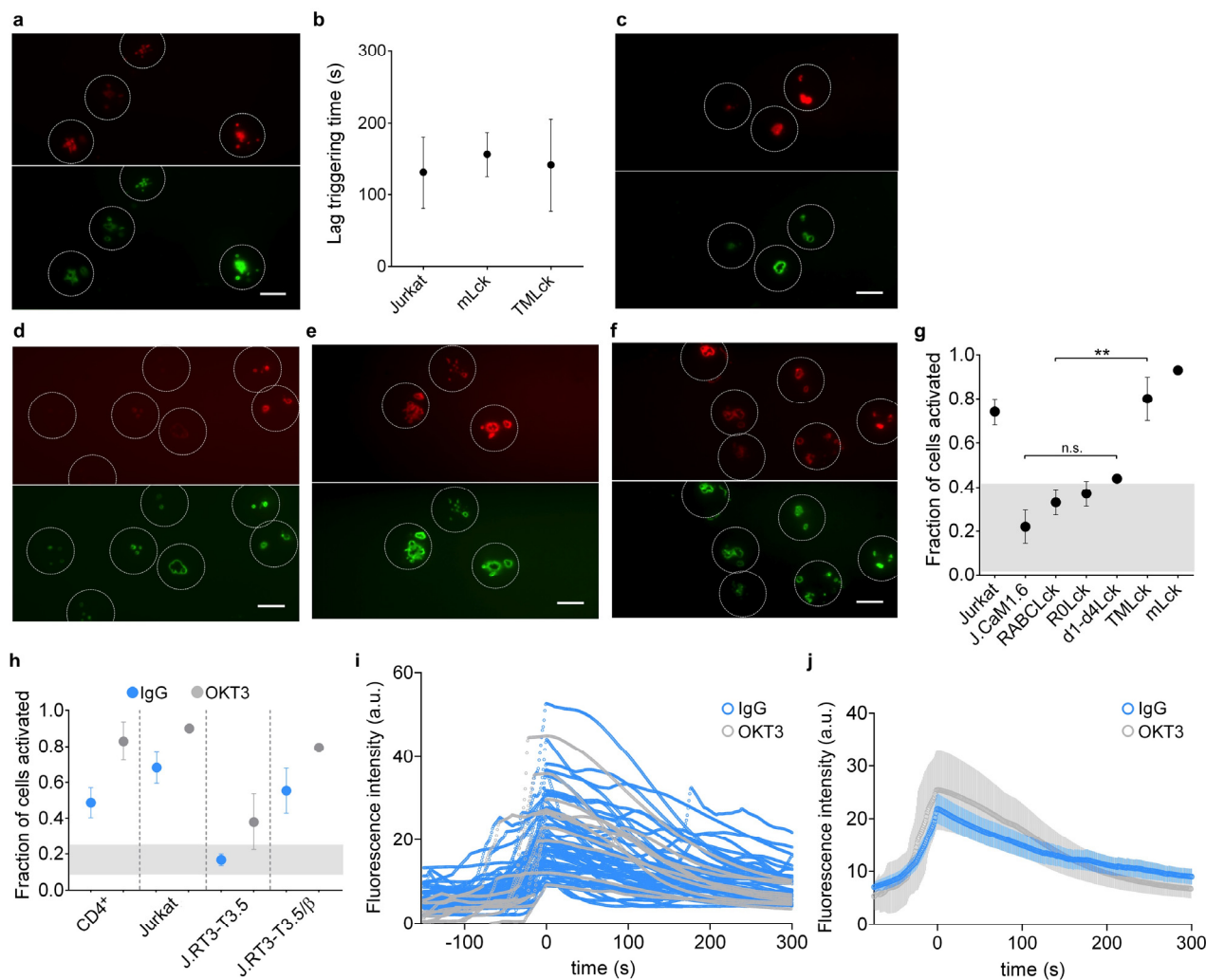




### Supplementary Figure 3

#### Electron microscopy.

**(a)** Examples of Sema6A-CD45R0 negative-staining EM raw images corresponding to each of the 50 classes shown in **(b)**. Each class contained between 127 and 399 such images. **(b)** Sema6A-CD45R0 negative-staining EM class averages. The gallery of all fifty class-sums derived from the Sema6A-CD45R0 images (*top*) and their corresponding I-images (*bottom*). **(c)** Fourier Shell Correlation of the reconstruction of Sema6A-CD45R0 made using SPIDER software, showing a resolution at FSC = 0.5 of 33 Å. **(d)** The original class averages of the Sema6A-CD45R0 negative stain images, prior to 3D reconstruction, compared to reprojections of the reconstruction itself. In each case the class averages are grouped by reference to the reprojections they agree with best. For each block of images (1–24), the final image (marked by yellow borders) is the reprojection best matching the other image(s) shown in that block. **(e)** Two views (as in Figure 3c of the main text) of the reconstruction fitted with the Sema6A and CD45d1–d4 region and with the mucin linker modeled in between them. Pairs of images are shown, in which the first is the same as in Figure 3c and the second has superimposed a map calculated for the Sema6A-CD45R0 atomic model filtered to 33 Å to show that the mucin linker is unresolved.



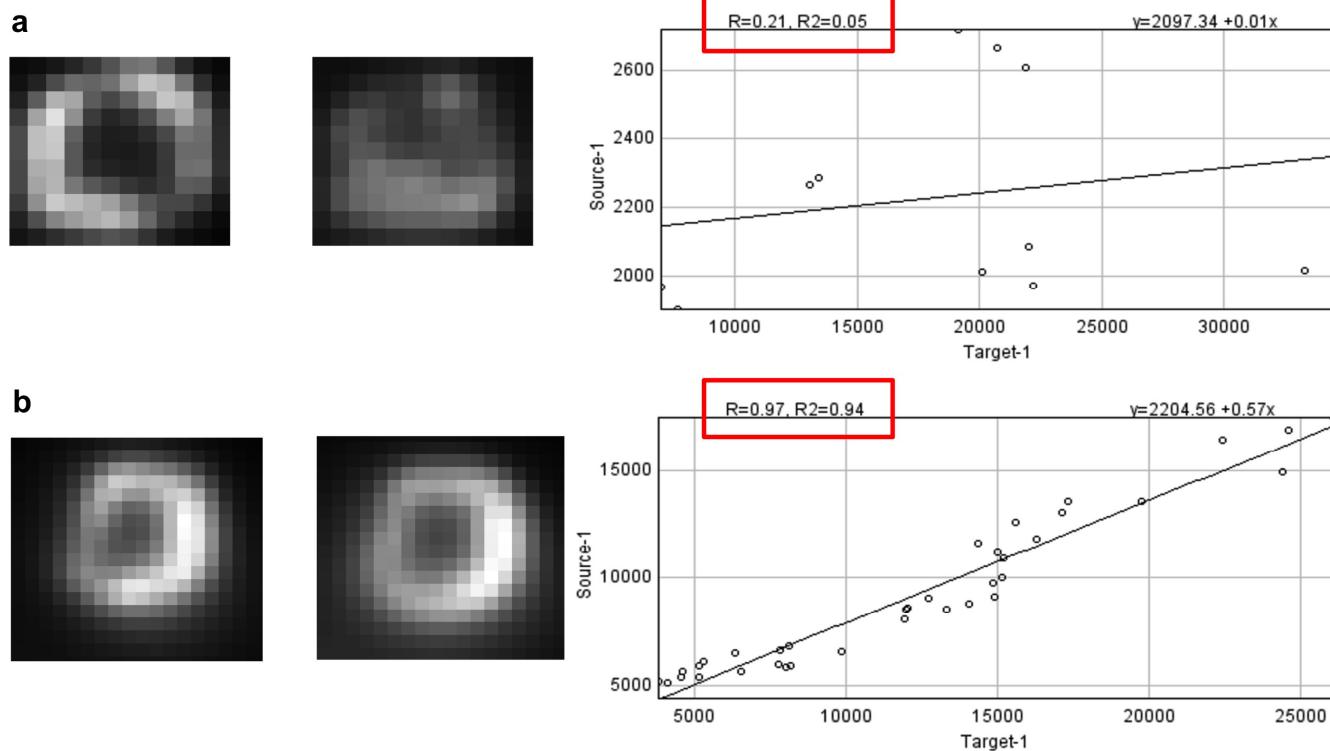
**Supplementary Figure 4**

#### **Distribution of non-chimeric and chimeric forms of Lck versus CD45 and signaling at close contacts.**

**(a)** Additional examples of close contact formation and CD45 segregation observed for J.CaM1.6 T cells expressing mLck. **(b)** Mean time taken between initial cell contact with OKT3-coated glass surface and calcium release (maximum Fluo-4 fluorescence signal; lag triggering time), at 20°C. **(c–f)** Additional examples of close contact formation and CD45 segregation observed for J.CaM1.6 T cells expressing TMLck (c), RABCLck (d), R0Lck (e) and d1–d4Lck (f) interacting with an OKT3-coated surface. The Lck constructs were labeled via a HaloTag and HaloTag TMR (red) and CD45 was labeled using Alexa Fluor 488-tagged Gap 8.3 Fab fragments (green). Cell positions were estimated from white-light transmission images (white circles). Imaging data in (a) and (c–f) was taken at 20°C; scale bars, 5  $\mu$ m. **(g)** Fractions of J.CaM1.6 T cells expressing the constructs shown in **Figure 5a,b** of the main text eliciting a calcium response upon contacting OKT3-coated glass at 37°C. Short-, but not the long-forms of Lck rescue OKT3-triggered signaling in J.CaM1.6 T cells. The shaded part of the graph is the 95% confidence interval for the J.CaM1.6 dataset

defining the range of values for individual calcium responses indistinguishable from those of the J.CaM1.6 cells. **(h)** Calcium responses of T cells contacting glass surfaces in the presence and absence of anti-TCR antibody. Glass surfaces were coated with OKT3 antibody or bovine IgG ("IgG"). The fractions of native CD4<sup>+</sup> ("CD4<sup>+</sup>") and normal or mutant Jurkat T cells expressing or not expressing the TCR that elicited a calcium response upon contacting the coated surfaces at 37°C are shown. The shaded part of the graph is the 95% confidence interval for the J.RT3-T3.5 dataset defining the range of values for individual calcium responses indistinguishable from those of the J.RT3-T3.5 cells. **(i)** Individual calcium (Fluo-4) intensity profiles for triggered cells contacting OKT3 or IgG-coated glass surfaces at 37°C. **(j)** Mean intensity profiles of 100 randomly chosen cells triggered in response to contacting OKT3 or IgG-coated glass surfaces at 37°C (mean ± S.D.). The data were collected in at least three independent experiments.

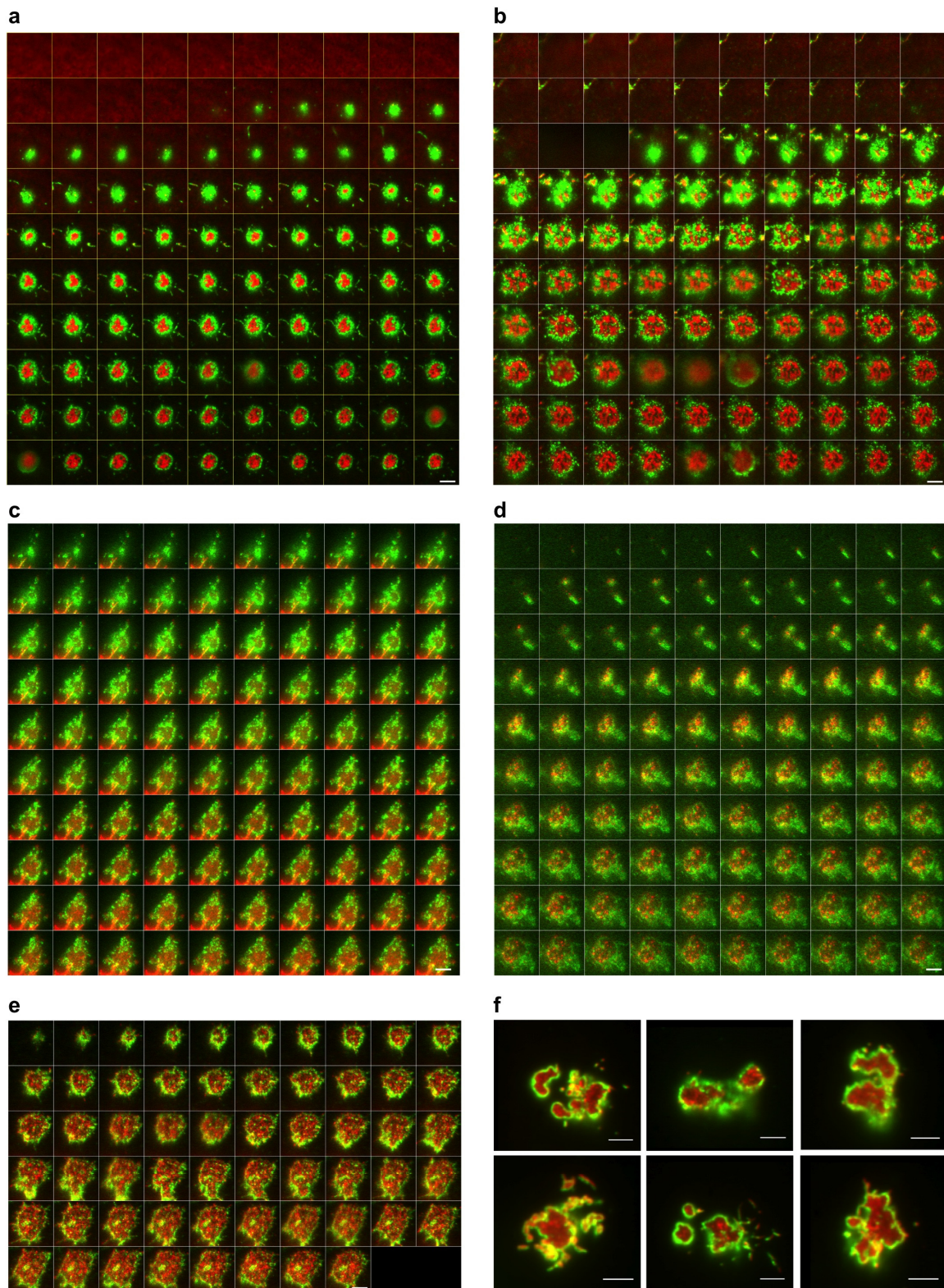




**Supplementary Figure 5**

**Principle of  $R^2$  analysis.**

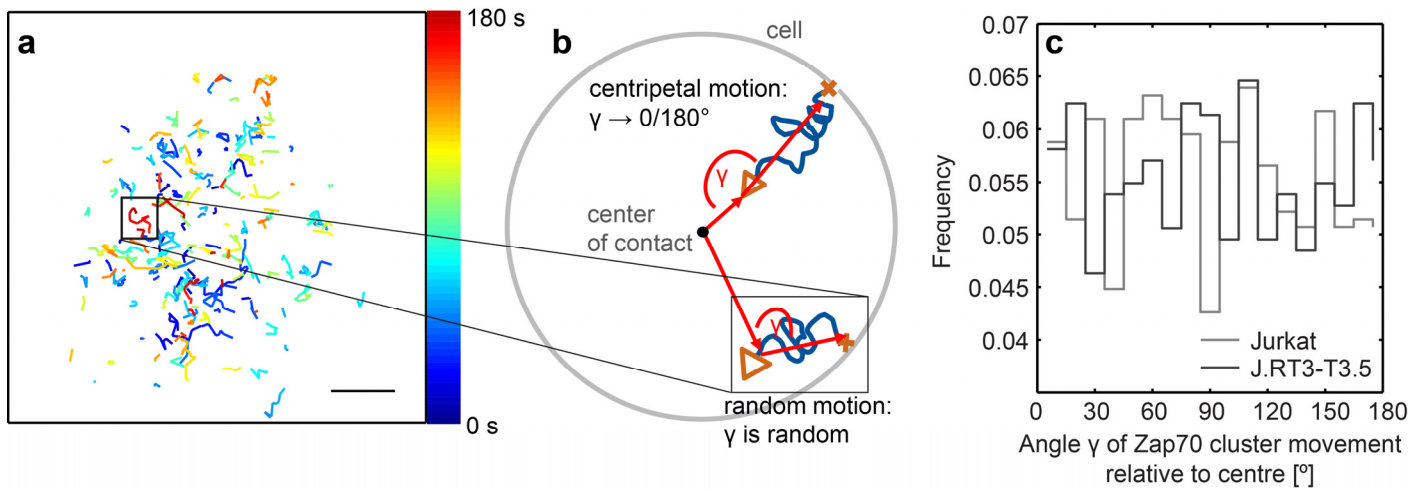
(**a**) Pixel intensities from images that are anti-correlated when plotted against each other display a poor linear fit, whereas correlated images (**b**) display a good fit.



## Supplementary Figure 6

### Close contacts formed with an SLB.

(**a**) Montage from a time-lapse showing the spatio-temporal organization of CD45 (labeled with Alexa Fluor 488-tagged Gap 8.3 Fab, green) during contact of a Jurkat T cell expressing a transmembrane-anchored, non-signaling, T92A-mutated form of CD48 (CD48<sup>+</sup>) and a SLB containing rCD2 (Alexa Fluor 647-tagged, red). (**b**) Equivalent to (**a**) except that the fluorophores are swapped (CD45 is labeled with Alexa Fluor 647-tagged Gap 8.3 Fab, green, and rCD2 is tagged with Alexa Fluor 488, red). (**c–e**) Montages show distribution of a truncated form of CD45 (HA-CD45, **c**), TCR (**d**) and mLck (**e**) each labeled with HaloTag TMR, red) versus CD45 (green) during contact of a CD48<sup>+</sup> Jurkat T cell with a SLB containing rCD2. The time intervals between frames shown are 5 s; data was collected at 37°C. (**f**) More examples of mLck versus CD45 distribution at T cell contacts with SLBs. Examples of rarer multi-focal contacts of CD48<sup>+</sup> Jurkat T cells with rCD2-containing SLBs showing the organization of CD45 (labeled with Alexa Fluor 488-tagged Gap 8.3 Fab, green) and mLck labeled with HaloTag TMR (red).



**Supplementary Figure 7**

**Non-centripetal motion of Zap70 clusters.**

(a) Zap70 cluster trajectories (colour-coded with time). (b) Schematic depiction of the trajectory analysis: the vector from the center of the contact to the end of a given trajectory is calculated as well as the vector from the start to the end of the trajectory. The angle between the two vectors is 0/180° for centripetal motion, and takes a random value for random motion. (c) Histogram showing the frequencies for all calculated angles  $\gamma$  for Zap70 trajectories observed in Jurkat and JRT3-T3.5 cells during the first 180 s post contact formation with a rCD2 bilayer. Total number of trajectories analyzed: 2234 (Jurkat), 2158 (JRT3-T3.5), total number of analyzed cells: 28 (Jurkat), 36 (JRT3-T3.5). The data were collected in at least three independent experiments.

**Supplementary Table 1**  
**Crystallographic data collection and refinement statistics**

	CD45d1d2	CD45d1d2	rCD45d3d4	rCD45d3d4	CD45d1–d3	CD45d1–d4
	native	KPtCl <sub>4</sub>	native	Ta <sub>6</sub> Br <sub>12</sub>	native	native
<b>DATA COLLECTION</b>						
X-ray source	ESRF-ID23EH1	ESRF-ID23EH1	Diamond-I03	Diamond-I02	ESRF-ID23EH2	Diamond-I041
Resolution	43.0–2.3 (2.36–2.30)	30.0–3.30 (3.42–3.30)	96.0–2.45 (2.52–2.45)	50.0–3.28 (3.40–3.28)	50.0–3.3 (3.42–3.30)	50.0–2.9 (2.98–2.90)
Space group	P6 <sub>3</sub>	P6 <sub>3</sub>	I222	I222	H3	P2 <sub>1</sub>
Cell dimensions	a = 146.6 Å b = 146.6 Å c = 52.7 Å	a = 149.2 Å b = 149.2 Å c = 52.3 Å	a = 84.4 Å b = 131.2 Å c = 141.3 Å	a = 84.0 Å b = 131.8 Å c = 141.3 Å	a = 132.4 Å b = 132.4 Å c = 58.1 Å	a = 94.6 Å b = 59.4 Å c = 100.4 Å β = 111.7°
Solvent content [%] (molecules per AU)	71 (2)	71 (2)	75 (2)	75 (2)	64 (1)	63 (2)
Unique reflections	30027 (2179)	10213 (1006)	29113 (2099)	12381 (1226)	5693 (579)	22973 (1684)
Completeness [%]	99.2 (99.8)	100 (100)	99.7 (99.5)	99.9 (99.9)	100.0 (100.0)	98.6 (97.7)
R <sub>merge</sub> [%]	8.5 (91.9)	17.6 (100)	4.7 (96.5)	9.2 (70.6)	25.8 (90.4)	8.8 (82.4)
I/σI	17.6 (2.6)	23.5 (3.5)	17.9 (1.5)	24.8 (3.8)	6.8 (2.0)	9.9 (1.5)
Redundancy	9.2 (9.1)	23.4 (23.7)	4.8 (4.1)	13.9 (13.7)	4.5 (4.5)	3.5 (3.5)
<b>REFINEMENT</b>						
Resolution range [Å]	40.0–2.3 (2.38–2.30)		30.7–2.45 (2.54–2.45)		41.0–3.3 (3.69–3.30)	50.0–2.9 (3.05–2.90)
Number of reflections	30020 (2927)		29106 (2804)		5687 (1597)	22584 (2713)
No. of atoms (protein/ /H <sub>2</sub> O/NAG/Hg/FLC/SO <sub>4</sub> )	2744/110/2 36/2/0/0		2822/56/14 0/0/13/0		2030/0/70/0/0/0	5632/0/154/0/0/25
B factors [Å <sup>2</sup> ] (protein/ /H <sub>2</sub> O/NAG/Hg/FLC/SO <sub>4</sub> )	57/56/90/12 0/-/-		80/75/103/- /125/-		63/-/70/-/-/-	106/-/109/-/-/95
R <sub>factor</sub> [%]	20.3 (24.8)		21.6 (27.0)		21.1 (23.1)	22.7 (26.0)
R <sub>free</sub> [%]	23.9 (27.4)		23.6 (27.3)		24.1 (29.0)	24.9 (29.5)
r.m.s.d. bonds [Å]§	0.010		0.010		0.009	0.010
r.m.s.d. angles [deg]	1.30		1.22		1.3	1.22
Ramachandran statistics						
Favoured [%]	97.1		94.6		95.2	96.7
Disallowed [%]	0		1.1		0.4	1.2

§ r.m.s.d.: root mean square deviation from ideal geometry. Numbers in parentheses refer to the appropriate outer shell.  
 AU: asymmetric unit. *R*<sub>free</sub> equals the *R*-factor against 5% of the data removed prior to refinement.



**Supplementary Table 2****Characterization of close contacts and CD45/Lck distribution**

Values from the data presented in **Figure 5e,f** for the “short” and “long” forms of Lck. Measurable contacts are defined as spatially isolated zones that are larger than the diffraction limit (as discussed in the Online Methods).

Construct	Total cells ( <i>n</i> )	Total contacts	Measurable contacts	Measurable fraction	Mean contacts per cell	$\sigma$	Coefficient of determination ( $R^2$ )	
mLck	52	299	99	0.33	5.75	$\pm 1.81$	0.53	$\pm 0.05$
TMLck	32	216	77	0.36	6.75	$\pm 1.58$	0.51	$\pm 0.06$
d1–d4Lck	48	348	111	0.32	7.25	$\pm 2.34$	0.98	$\pm 0.02$
R0Lck	24	121	44	0.36	5.04	$\pm 1.27$	0.79	$\pm 0.07$
RABCLck	25	112	38	0.34	4.48	$\pm 0.87$	0.82	$\pm 0.12$